PREPARATION OF A NOVEL CLAY/DYE COMPOSITE AND ITS APPLICATION IN CONTAMINANT DETECTION

Limei Wu[1], Xuyuan Bao[2], Haoyu Zhong[1], Yuwei Pan[1], Guocheng Lv[3]*, and Libing Liao[3]

[1]School of Materials Science and Engineering, Shenyang Jianzhu University, Shenyang 110168, China
[2]The Beijing Municipal Key Laboratory of New Energy Materials and Technologies, School of Materials Sciences and Engineering, University of Science and Technology Beijing, Beijing 100083, China
[3]Beijing Key Laboratory of Materials Utilization of Nonmetallic Minerals and Solid Wastes, National Laboratory of Mineral Materials, School of Materials Science and Technology, China University of Geosciences, Beijing 100083, China

Abstract—Although fluorescence detection is a sensitive method in the field of pollutant analysis, its application is restricted due to the fluorescence shown by organic material being quenched after aggregation and to low photo-thermal stability. To address these issues, a novel mineral/dye composite material was prepared by intercalating a fluorescence molecule, Rhodamine (R6G), into the interlayer space of montmorillonite (Mnt). This composite material greatly enhanced the light stability and efficiency of R6G. After enhancement, the fluorescence lifetime of R6G-Mnt was eight times longer than originally and the luminous intensity was 20 times greater. Chromium at the mmol/L (mM) level can be detected by the naked eye when its enhanced fluorescent property is fabricated into a solid test paper, even though a fluorescence spectrophotometer should be used for detection at the 0.01 μmol/L level in the sensing range 0.01 μmol/L to 100 mmol/L. These results can provide new avenues as well as a theoretical and experimental foundation for the development of novel supramolecular luminescent material.

Keywords—Detection · Fluorescence quenching · Inorganic/organic composite · Light-emitting efficiency

INTRODUCTION

Fluorescent materials and their derivatives are used widely, especially in functional materials, such as: pH test strips, formaldehyde test kits, etc., as well as in biological and medical fields (Haugland 1994). The broad applications of organic fluorescent materials in diverse areas are due to their flexible structures (Skaff et al. 2004; Zhang et al. 2005). Several dye compounds can be used in the luminous field; their applications, however, are limited by multiple drawbacks (*e.g.* concentration quenching and low-light thermal stability in the solid state) (Lee et al. 2000; Zhang et al. 2003).

Chromium (Cr) compounds are used widely in various sectors of industry (Mondal 2009; Olmez 2009). Cr is a major industrial pollutant and its concentration in the environment keeps increasing due to its extensive use in leather tanning, stainless-steel production, and electroplating (Lalvani et al. 1998; Kantar et al. 2008). A rapid and efficient way to detect Cr(VI) is, therefore, crucial in the development of water contaminant treatment. Detection of Cr(VI) is most commonly performed by using atomic absorption spectroscopy, inductively coupled plasma mass spectrometry, and electrochemical methods (Sperling et al. 1992; Powell et al. 1995; Zheng et al. 2013). Many of these methods are sensitive and accurate, but they are also costly and require sophisticated instrumentation. A clear, unmet need exists for sensitive, specific, and selective detection and quantification of Cr(VI). Fluorescence spectroscopy is used increasingly, due to its sensitivity compared to other

techniques (Nolan & Lippard 2008) and, coupled with organic and inorganic semiconducting luminescent materials, have shown great promise (George et al. 2014).

Fluorescent chemical sensing materials and their applications have been a focus for some time in interdisciplinary research (Zheng et al. 2003; Shi et al. 2005; Austin et al. 2018). Fluorescent chemical sensing materials use probe molecules to form chemical bonds or supramolecular interactions with target molecules, quenching or enhancing the fluorescence of the molecules. Hence, easy, highly sensitive detection of target molecules or ions is achieved (Patra & Mishra 2002). For instance, the detection limit of phenol can be as low as 1 μM (Sergeyeva et al. 2014). All detection of contaminants should be carried out under the same conditions, however (Goswami et al. 2013; Bao et al. 2014; Lee et al. 2014); organic solvents used in the process also cause environmental problems (Ego et al. 2003).

The use of weak interaction forces (hydrogen bond, hydrophobicity, Van der Waals force, π-π, and static electricity) between the inorganic molecules (host) and organic probe molecules (guest) to formulate inorganic-organic hybrid fluorescent chemical materials has been studied previously (see, for example, Karataş et al. 2017). The process of supramolecular formulation is simple and widely applicable (Gao et al. 2012). Layered, two-dimensional nano-materials have large specific surface areas and homogeneous surface properties, and tend to form multi-layer structures in supramolecular formulations because of their large cation exchange capacity (CEC), and, to a certain extent, pseudo-agglomeration of probe molecules. These advantages facilitate layered two-

---

dimensional nano-materials as a host prior to the formulation of inorganic-organic fluorescent materials. Clay minerals provide distinct nanometer-scaled layers and interlayers for engineering as selective and active adsorbents and catalysts (Zhou et al. 2016). As a vital clay mineral, montmorillonite (Mnt) is a 2:1 phyllosilicate mineral that consists of layered silicon tetrahedral and aluminum octahedral sheets with negatively charged layers compensated by cations, such as Na^+ and Ca^{2+} (Whitney & Evans 2010; Wu et al. 2014a). Mnt has a large CEC; the cations can thus be replaced by other inorganic or organic cations. This is an effective way to construct ordered inorganic-organic and inorganic-inorganic assemblies with unique microstructures and properties. The Mnts have attractive properties, including large specific surface area, swellability, adsorption capacity, and cation exchange capacity. These features facilitate the formulation of fluorescent molecules in Mnt interlayer spaces and, thereby, provide good potential for the development of fluorescent sensor materials for the detection of trace contaminants. The electrostatic charge on the layers plays a leading role in the attraction between clay minerals and organic material (Čeklovský et al. 2009; An et al. 2015; Zhou et al. 2019).

The objective of the current study was to use clay/organic intercalation composites as novel fluorescent materials, fabricated by the controlled assembly of fluorescent molecules into the Mnt interlayer, to achieve sensitive detection of trace Cr(VI) in water (Fig. 1) These composites have greater sensitivity than the 7-amino-4-methylcoumarin/montmorillonite composite fabricated by Wei et al. (2018). The hypothesis was that the outcomes would add more fundamental understanding of the assembly mechanisms for guest–host interactions and would provide novel ideas for future development and applications of sensing materials.

EXPERIMENTAL AND METHODS

Montmorillonite (SWy-2) was obtained from the Source Clays Repository of The Clay Minerals Society. Details of the Mnt were given by Wu et al. (2014a).

Rhodamine 6G (R6G) is a catechol compound (Fig. 2) which possesses a large degree of conjugation. It is a red or yellowish brown powder, soluble in water. R6G aqueous solution is scarlet in color, with a green fluorescence. The R6G molecule is 12.5 Å wide and 7.14 Å high. The initial concentrations of R6G varied from 0.1 to 10.5 mM for the adsorption isotherm study. The R6G-Mnt was prepared by the method of Lv et al. (2018).

A UV-Vis spectrophotometer (SPECORD 50 plus, made by Analytik Jena AG, Beijing, China) operated at a wavelength of 527 nm was used to analyze the equilibrium R6G concentrations. Powder XRD analyses were performed using a Rigaku D/max-IIIa diffractometer (Tokyo, Japan) with Ni-filtered CuKα radiation at 30 kV and 20 mA. The data for orientated samples were

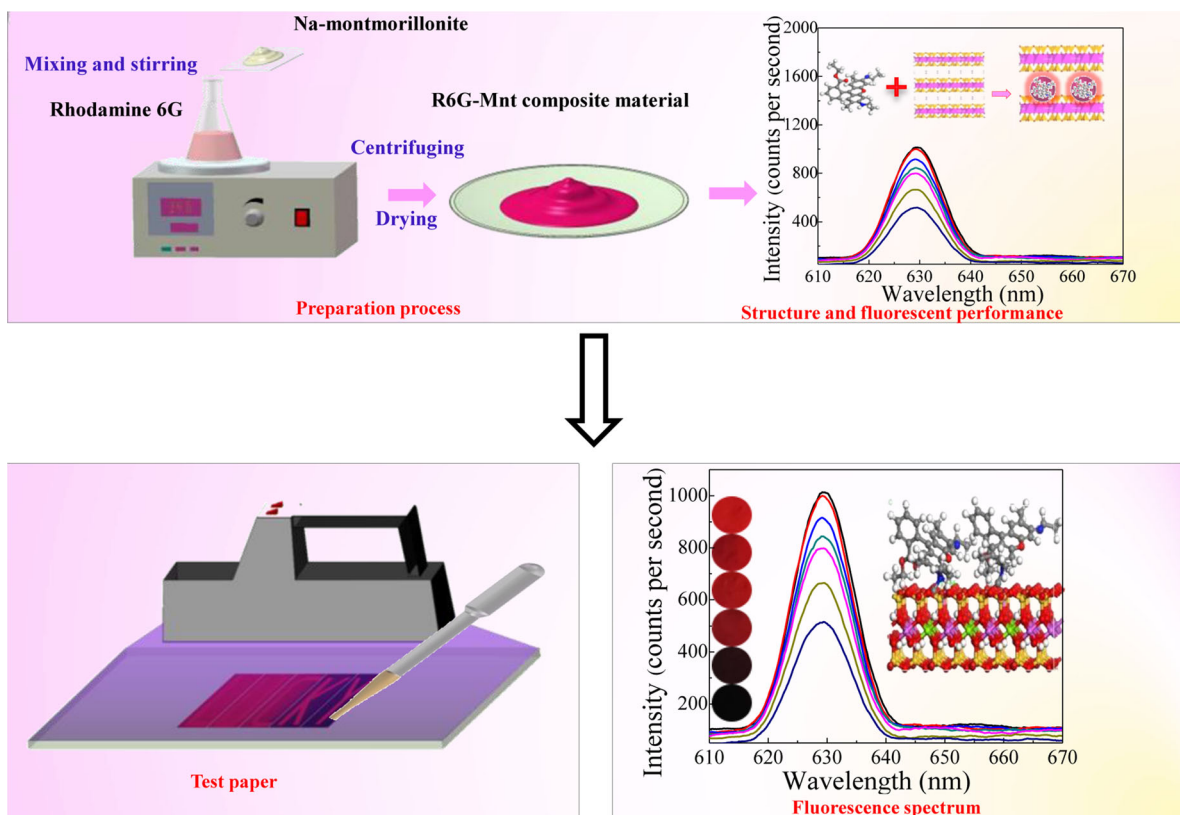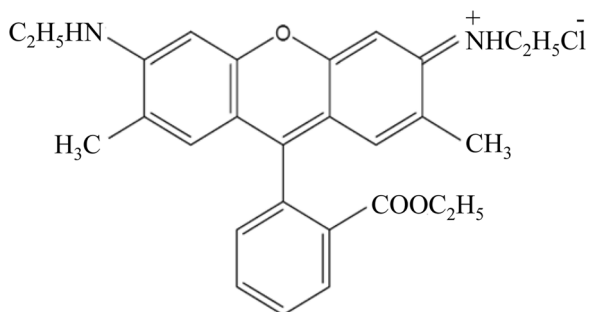**Fig. 1.** Schematic view of the preparation of R6G -Mnt and the detection of Cr(VI)

Fig. 2 The structure of R6G

collected over the range (3°–70°2θ) with a scanning step of 0.01°2θ and a scanning speed of 2°2θ/min. A fluorescence spectrophotometer (HITACHI, F4600, Beijing, China) with a photomultiplier tube operating at 400 V and an excitation source with a 150 W xenon lamp was used to measure the photoluminescence excitation (PLE) and emission (PL) spectra. The lifetimes were recorded on a spectro-fluorometer (HORIBA, JOBIN YVON FL3-21, Edinburgh, UK) with a 210 nm pulse laser radiation (nano-LED) as the excitation source.

Molecular simulation was carried out under the module *CASTEP* of *Materials Studio* 6.0 software to study the configuration of the uptake of R6G by Mnt (Wu et al. 2014a). The unit-cell parameters were $a = 15.540$ Å, $b = 17.940$ Å, $c = 12.56$ Å, $\alpha = \gamma = 90°$, and $\beta = 99°$. A series of $(3\times2\times1)$ supercells was built with the layer spacing set at 15.08 and 20.45 Å for Mnt and R6G-Mnt, respectively.

RESULTS AND DISCUSSION

Preparation and Characterization of R6G-Mnt Luminescent Composites

Rhodamine (R6G) has a pKa value of 7.5 (Khurana & Santiago 2009); as the equilibrium solution pH value was
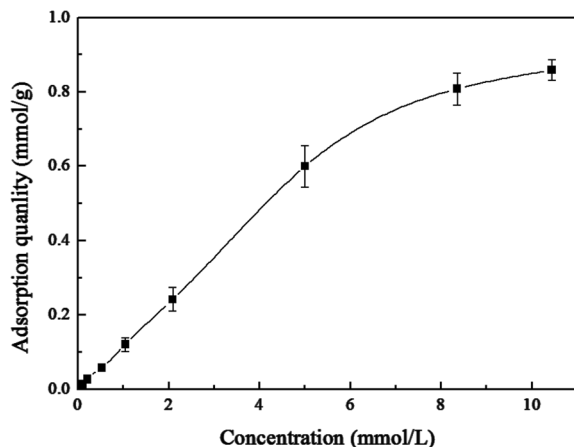

Fig. 3. Adsorption curves of rhodamine by montmorillonite (R6G-Mnt)
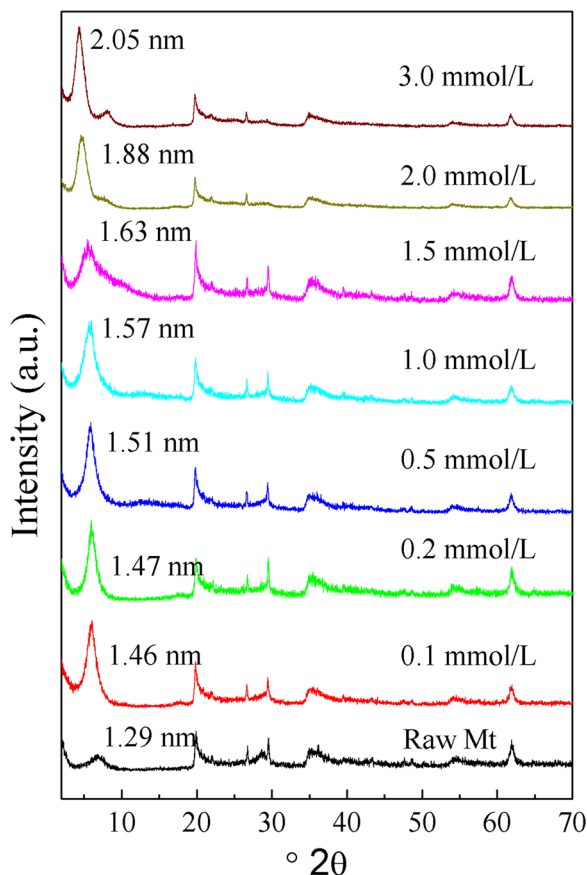

Fig. 4. X-ray diffraction patterns of R6G-Mnt at various concentrations of R6G

~3–5, most of the R6G existed as a monovalent cation (Zhang et al. 2011; Lee et al. 2015). The amount of R6G adsorbed by Mnt increased as the concentration of the solution increased (Fig. 3). The adsorption capacity increased sharply when the concentration of R6G was ~0.1–5 mM, and then showed a slow increase when the concentration of R6G was >5
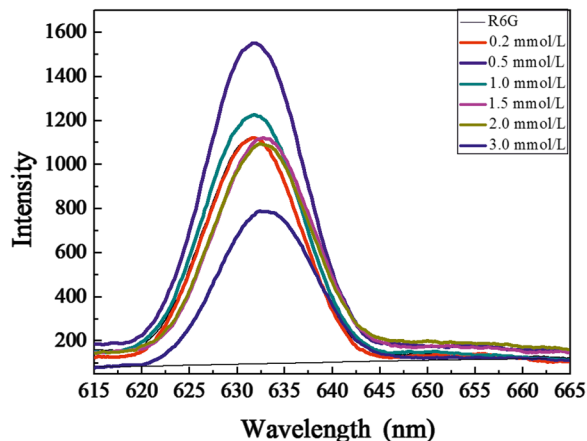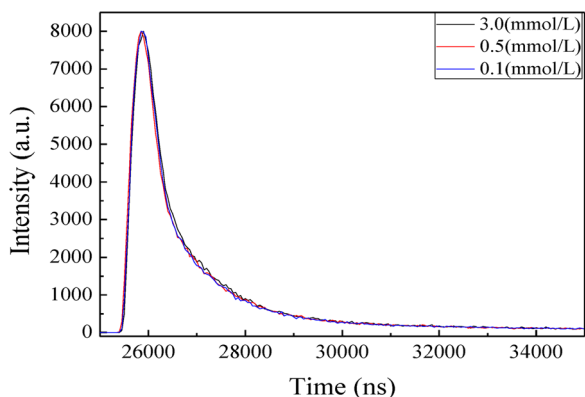

Fig. 5 Fluorescence spectra of the R6G and R6G-Mnt

Fig. 6. Fluorescence decay curves of R6G-Mnt

mM. When the concentration was 8 mM, the adsorption reached a balance point and the amount of RG6 intercalated into Mnt showed a maximum value of 0.8 mmol/g. This indicates that the amount of R6G intercalated into Mnt is related to the amount of R6G adsorbed by Mnt . The intercalation quantity affects the distribution of R6G in the interlayer space of Mnt (Wu et al. 2014a).

The degree of intercalation by R6G is reflected by the d_{001} value of R6G-Mnt as determined by XRD. The interlayer spacing of Mnt was related to the initial concentration of R6G solution. R6G replaced Na as the interlayer cation, and thus increased the d_{001} spacing (Fig. 4) from an initial value of 1.29 nm to 1.58 nm when the initial concentration of R6G was 0.1 mM, and reached a maximum value (2.05 nm) when the concentration of R6G was 3 mM. The trend for the basal spacing (d_{001}) was the same as that for the interlayer space. The different properties of R6G-Mnt were due to the different incorporation and arrangement of intercalation (Wu et al. 2014b). The results confirm that the hydrophobic force among alkyl chains of organic cations is the driving force for their intercalation (Dultz et al. 2005; Klebow & Meleshyn 2012; Yu et al. 2017).
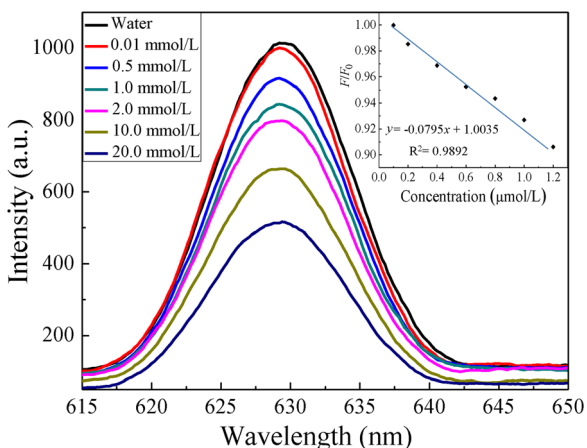

Fig. 7. Fluorescence spectra of R6G-Mnt in an aqueous buffer in the presence of various concentrations of chromium. Inset: fluorescence intensity ratio (F/F_0) changes at 527 nm

The intercalation of R6G into Mnt not only affected the interlayer spacing but also the arrangement of interlayer R6G and its interaction force with the Mnt layer. Pure R6G has an extremely low luminous intensity because of the concentration quenching effect; after being intercalated into the interlayer of Mnt, the luminous intensity was notably improved. In the emission spectrum of R6G at different amounts of intercalation (Fig. 5), when the initial concentration of R6G solution was 0.5 mM, R6G-Mnt had its greatest spectral intensity. At other concentrations, spectral intensities were lower, indicating that too much or too little intercalation of R6G reduced the luminous intensity of R6G-Mnt.

The lifetime of a luminous material is an indicator of its stability. The lifetime of R6G is only 4.1 ns (Magde et al. 2002); this improves significantly after intercalation into Mnt (Fig. 6). At an initial concentration of 0.5 mM, R6G had the longest lifetime (31.12 ns), which is almost eight times greater than that of the original and better than other assembly techniques (Yan et al. 2011a; Yan et al. 2011b). The interactions between the Mnt layer and the interlayer R6G, which had a supramolecular structure, had a significant effect on the lifetime and aging resistance of R6G. The results of this study may solve the problems of low thermal stability and short lifetime in the application of organic luminous molecular devices (Wu et al. 2015a, 2015b).

Cr(VI) Detection in Aqueous Phase by R6G-Mnt

Good fluorescence makes R6G-Mnt a suitable fluorescent detector of contaminants. The addition of Cr(VI) triggered an apparent quenching of the R6G-Mnt peak (Fig. 7). When the concentration of Cr(VI) was increased from 0 to 20 mM, a gradual reduction in the PL spectrum was observed. When the concentration of Cr(VI) was 20 mM, the PL spectrum was half what it was when the concentration was 0.0 mM. Reduction in Cr(VI) led to a regular increase in PL spectra in conjugates and the fluorescence intensity ratio (F/F_0) varied linearly with the addition of Cr(VI) in the range 0.01–1.2 μM ($R^2 = 0.9892$) (Fig. 7 inset). R6G has a lower detection limit than the 7-amino-4-methylcoumarin/montmorillonite composite (Wei et al. 2018). For this proposed method, the limit of detection (LOD) was 10.08 ± 0.11 nM, which was calculated using $3\sigma/k$ (where σ is the standard deviation for six replicating detections of blank solutions and k is the slope of the calibration curve) (Wu & Yan 2010; Lv et al. 2018) and was better than that of other related single-intensity-based PL sensors (Xu et al. 2011; Gui et al. 2012; Irannajad & Haghighi 2017).

To compare the detecting efficiency of R6G-Mnt for several typical cationic contaminants, R6G-Mnt was made into round disks with a diameter of 1 cm and placed in Cr(VI), Fe(III), and Cu(II) solutions with various concentrations (Table 1). The fluorescence quenching of R6G-Mnt increased with increase in Cr(VI) concentration. When Cr(VI) solution (0~100 mM) was added to an R6G-Mnt wafer, the increase in fluorescence quenching could be distinguished by the naked eye. These results suggest that Cr(VI) induced PL quenching of conjugates with high selectivity. The fluorescence intensity in images of R6G-Mnt following addition of Cr(VI) under

Table 1 Image of R6G-Mnt in aqueous buffer in the presence of various concentrations of Cr^{6+}, Fe^{3+}, and Cu^{2+}

Concentration (mmol/L)	0.0	0.1	2.0	5.0	20.0	100.0
Cr^{6+}						
Fe^{3+}						
Cu^{2+}						

fluorescent light decreased as the chromium concentration increased (Fig. 8). Next, R6G-Mnt was made into a test paper to examine luminescence when various concentrations of Cr(VI) solution interacted with R6G-Mnt. The examination showed quick and accurate detection of Cr(VI) by R6G.

Mechanism of Detection of Cr(VI) by R6G-Mnt

The interlayer spacing of Mnt plays a crucial role in the system's structure and interaction forces (Tong et al. 2006; Krauss et al. 2011; Wang et al. 2011). Mnt with the interlayer R6G arranged in a parallel fashion has a smaller interlayer spacing than Mnt with R6G tilted or vertical. (Fig. 9). Taking into account the amount of intercalated R6G and the change in the Mnt interlayer spacing, the orientation distances of $-N^+$ groups to the Mnt layer were calculated by molecular simulation for various intercalation amounts and interlayer distance. At concentrations of 0.5 mM and 3 mM, the numbers of intercalated molecules in Mnt were 2 and 4, respectively, and the corresponding arrangements of R6G in the Mnt space were tilted monolayer and tilted bilayer, respectively, while the distances of $-N^+$ groups from the Mnt layer were 1.446 and 1.887 Å,

respectively. Based on these results, the luminescence of R6G-Mnt was related to the amount of R6G intercalated into Mnt and also to the arrangement of R6G in Mnt space. Pure R6G showed poor luminescence because of the concentration quenching effect. Similarly, when the amount of R6G intercalated was >0.4 mmol/g, the intermolecular force could increase and concentration quenching also occurred (Montalti et al. 2002). A large concentration (>0.3 mmol/L) of R6G caused a stronger interaction force between molecules, leading to quenching. The molecule-end amino twirling aggravated internal conversion, broke the rigid plane of oxygen in the heteroanthracine parent ring, and consequently reduced the production of fluorescence quanta. For relatively small amounts (<0.2 mmol/g) intercalated, R6G molecules were restricted and distributed evenly in Mnt space, which led to a separation of R6G molecules from each other, reduced the intermolecular force, and prevented concentration quenching. When the intercalation of R6G into Mnt was 0.08 mmol/g and R6G was distributed uniformly in the interlayer, the luminescence of R6G -Mnt composite was at a maximum.

Fig. 8. Images of R6G-Mnt with various concentrations of chromium under ultraviolet light. The contrast between the letters and the background becomes stronger as the chromium concentration increases
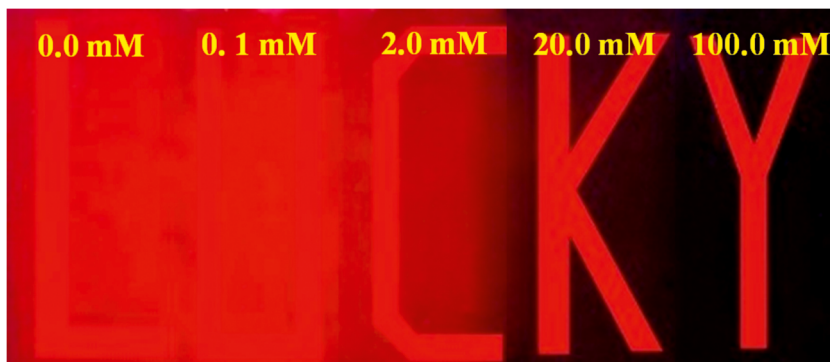
Fig. 9 Molecular dynamics simulation of intercalation for various arrangements of R6G in Mnt. For all species, C = gray, N = blue, H = white, O = red, Si = yellow, Al = pink, and Mg = green
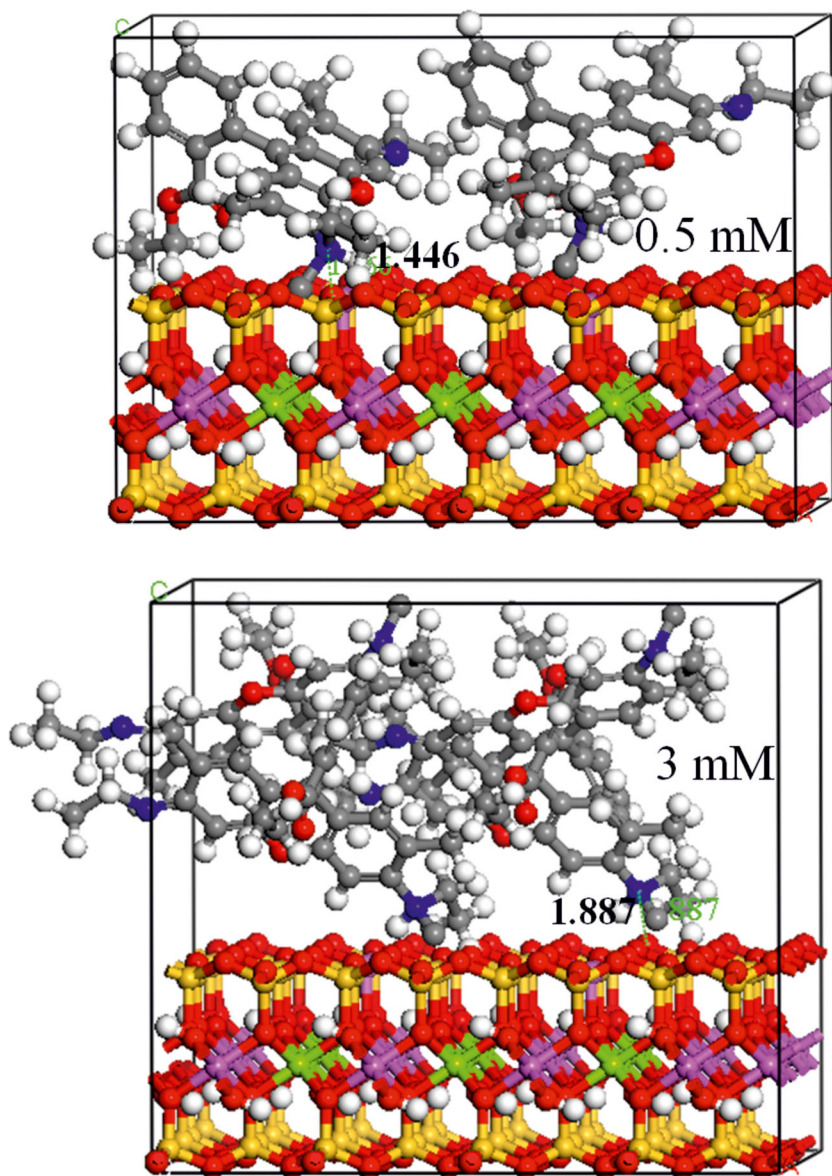
CONCLUSIONS

In summary, a novel supramolecular structure was constructed by intercalating R6G into Mnt. The R6G-Mnt composite exhibited significantly improved luminescence properties, including strong luminescence intensity and long lifetime, which indicates that R6G-Mnt may have potential applications in display and lighting devices. The introduction of Cr(VI) caused quenching of R6G-Mnt fluorescence, resulting in a high sensitivity to, and low detection limit of, Cr(VI). The outcome of this study provides more fundamentals for comprehension of the mechanism of guest–host interactions in the assembly, future development, and application of sensing materials.

ACKNOWLEDGMENTS

Conflict of Interest

There are no conflicts of interest to declare.

REFERENCES

An, N., Zhou, C. H., Zhuang, X. Y., Tong, D. S., & Yu, W. H. (2015). Immobilization of enzymes on clay minerals for biocatalysts and biosensors. *Applied Clay Science, 114*, 283–296.

Austin, J. C., Perry, A., Richter, D. D., & Schroeder, P. A. (2018). Modifications of 2:1 clay minerals in kaolinite-dominated ultisol under changing land-use regimes. *Clays and Clay Minerals, 66*, 61–73.

Bao, X., Shi, J., Nie, X., Zhou, B., Wang, X., Zhang, L., Liao, H., & Pang, T. (2014). A New Rhodamine B-based "on–off" chemical sensor with high selectivity and sensitivity toward Fe^{3+} and its imaging in living cells. *Bioorganic & Medicinal Chemistry, 22*, 4826–4835.

Bumbudsanpharoke, N., Lee, W., Choi, J. C., Park, S. J., Kim, M., & Ko, S. (2017). Influence of montmorillonite nanoclay content on the optical, thermal, mechanical, and barrier properties of low-density polyethylene. *Clays and Clay Minerals, 65*, 387–397.

Čeklovský, A., Czímerová, A., Lang, K., & Bujdák, J. (2009). Effect of the layer charge on the interaction of porphyrin dyes in layered silicates dispersions. *Journal of Luminescence, 129*, 912–918.

Dultz, S., Riebe, B., & Bunnenberg, C. (2005). Temperature effects on iodine adsorption on organo-clay minerals: II. Structural effects. *Applied Clay Science, 28*, 17–30.

Ego, C., Marsitzky, D., Becker, S., Zhang, J., Grimsdale, A. C., Müllen, K., Mackenzie, K., Silva, C., & Friend, R. H. (2003). Attaching perylene dyes to polyfluorene: Three simple, efficient methods for facile color tuning of light-emitting polymers. *Journal of the American Chemical Society, 125*, 437–443.

Gao, F., Ye, Q., Cui, P., & Zhang, L. (2012). Efficient fluorescence energy transfer system between CdTe-doped silica nanoparticles and gold nanoparticles for turn-on fluorescence detection of melamine. *Journal of Agricultural and Food Chemistry, 60*, 4550–4558.

George, S. J., Rao, K. V., & Jain, A. (2014). Organic–inorganic light-harvesting scaffolds for luminescent hybrids. *Journal of Materials Chemistry C, 2*, 3055–3064.

Goswami, S., Paul, S., & Manna, A. (2013). Selective "Naked Eye" detection of Al(III) and PPi in aqueous media on a rhodamine–isatin hybrid moiety. *RSC Advances, 3*, 10639–10643.

Gui, R., An, X., Su, H., Shen, W., Chen, Z., & Wang, X. (2012). A near-infrared-emitting CdTe/CdS Core/shell quantum dots-based off–on fluorescence sensor for highly selective and sensitive detection of Cd^{2+}. *Talanta, 94*, 257–262.

Haugland, R.P. (1994). *Molecular probes: Handbook of Fluorescent Probes and Research Chemicals*. International Union of Biochemistry and Medical Biology, Amsterdam.

Irannajad, M., & Haghighi, H. K. (2017). Removal of Co^{2+}, Ni^{2+}, and Pb^{2+} by manganese oxide-coated zeolite: Equilibrium, thermodynamics, and kinetics studies. *Clays and Clay Minerals, 65*, 52–62.

Kantar, C., Cetin, Z., & Demiray, H. (2008). In situ stabilization of chromium (VI) in polluted soils using organic ligands: The role of galacturonic, glucuronic and alginic acids. *Journal of Hazardous Materials, 159*, 287–293.

Karataş, D., Tekin, A., & Çelik, M. S. (2017). Density functional theory computation of organic compound penetration into sepiolite tunnels. *Clays and Clay Minerals, 65*, 1–13.

Khurana, T. K. & Santiago, J. G. (2009). Effects of carbon dioxide on peak mode isota-chophoresis: Simultaneous preconcentration and separation. *Lab on a Chip, 9*, 1377–1384.

Klebow, B. & Meleshyn, A. (2012). Monte carlo study of the adsorption and aggregation of alkyl trimethylammonium chloride on the montmorillonite−water interface. *Langmuir, 28*, 13274–13283.

Krauss, T. N., Barrena, E., Lohmuller, T., Spatz, J., & Dosch, P. H. (2011). Growth mechanisms of phthalocyanine nanowires induced by Au nanoparticle templates. *Physical Chemistry Chemical Physics, 13*, 5940–5944.

Lalvani, S. B., Wiltowski, T., Hubner, A., Weston, A., & Mandich, N. (1998). Removal of hexavalent chromium and metal cations by a selective and novel carbon adsorbent. *Carbon, 36*, 1219–1226.

Lee, I. H., Jang, L. W., & Polyakov, A. Y. (2015). Performance enhancement of GaN-based light emitting diodes by the interaction with localized surface plasmons. *Nano Energy, 13*, 140–173.

Lee, J., Sundar, V. C., Heine, J. R., Bawendi, M. G., & Jensen, K. F. (2000). Full color emission from II-VI semiconductor quantum dot-polymer composites. *Advanced Materials, 12*, 1102–1105.

Lee, Y. J., Lim, C., Suh, H., Song, E. J., & Kim, C. (2014). A Multifunctional sensor: Chromogenic sensing for Mn^{2+} and fluorescent sensing for Zn^{2+} and Al^{3+}. *Sensors and Actuators B: Chemical, 201*, 535–544.

Lv, G. C., Liu, S. Y., Liu, M., Liao, L. B., Wu, L. M., Mei, L. F., Li, Z. H., & Pan, C. F. (2018). Detection and quantification of phenol in liquid and gas phases using a clay/dye composite. *Journal of Industrial and Engineering Chemistry, 62*, 284–290.

Magde, D., Wong, R., & Seybold, P. G. (2002). Fluorescence quantum yields and their relation to lifetimes of rhodamine 6G and fluorescein in nine solvents: Improved absolute standards for quantum yields. *Photochemistry and Photobiology, 75*, 327–334.

Mondal, M. K. (2009). Removal of Pb(II) ions from aqueous solution using activated tea waste: Adsorption on a fixed-bed column. *Journal of Environmental Management, 90*, 3266–3271.

Montalti, M., Prodi, L., Zaccheroni, N., & Falini, G. (2002). Solvent-induced modulation of collective photophysical processes in fluorescent silica nanoparticles. *Journal of the American Chemical Society, 124*, 13540–13546.

Nolan, E. M., & Lippard, S. J. (2008). Tools and tactics for the optical detection of mercuric ion. *Chemical Reviews, 108*, 3443–3480.

Olmez, T. (2009). The optimization of Cr(VI) reduction and removal by electrocoagulation using response surface methodology. *Journal of Hazardous Materials, 162*, 1371–1378.

Patra, D. & Mishra, A. K. (2002). Recent developments in multi-component synchronous fluorescence scan analysis. *Trends in Analytical Chemistry, 21*, 787–798.

Powell, M. J., Boomer, D. W., & Wiederin, D. R. (1995). Determination of chromium species in environmental samples using high-pressure liquid chromatography direct injection nebulization and inductively coupled plasma mass spectrometry. *Analytical Chemistry, 67*, 2474–2478.

Sergeyeva, T., Chelyadina, D., Gorbach, L., Brovko, O., Piletska, E., Piletsky, S., Sergeeva, L., & Elskaya, A. (2014). Colorimetric biomimetic sensor systems based on molecularly imprinted polymer membranes for highly-selective detection of phenol in environmental samples. *Biopolymers and Cell, 30*, 209–215.

Shi, L., Wang, Y., Ji, A., Gao, L., & Wang, Y. (2005). In situ direct bifunctionalization of mesoporous silica SBA-15. *Journal of Materials Chemistry, 15*, 1392–1396.

Skaff, H., Sill, K., & Emrick, T. J. (2004). Quantum dots tailored with poly (para-phenylene vinylene). *Journal of the American Chemical Society, 126*, 11322–11325.

Sperling, M., Xu, S., & Welz, B. (1992). Determination of chromium(III) and chromium(VI) in water using flow injection on-line preconcentration with selective adsorption on activated alumina and flame atomic absorption spectrometric detection. *Analytical Chemistry, 64*, 3101–3108.

Tong, W. Y., Djurisić, A. B., Xie, M. H., Ng, A. C. M., Cheung, K. Y., Chan, W. K., Leung, Y. H., Lin, H. W., & Gwo, S. J. (2006). Metal phthalocyanine nanoribbons and nanowires. *Journal of Physical Chemistry B, 110*, 17406–17413.

Wang, F. X., Liu, Y. D., & Pan, G. B. (2011). Vapor growth and photoconductivity of single-crystal nickel-phthalocyanine Nanorods. *Materials Letters, 65*, 933–936.

Wei Y. K., Mei L. F., Li R., Liu M., Lv G. C., Weng J. L., Liao L. B., Li Z. H., & Lu L. (2018). Fabrication of an AMC/MMT fluorescence composite for its detection of Cr(VI) in water. *Frontiers in Chemistry, 6*, 367.

Whitney, D. L. & Evans, B. W. (2010). Abbreviations for names of rock-forming minerals. *American Mineralogist, 95*, 185–187.

Wu, L. M., Liao, L. M., Lv, G. C., Qin, F. X., & Li, Z. H. (2014a). Microstructure and process of intercalation of imidazolium ionic liquids into montmorillonite. *Chemical Engineering Journal, 236*, 306–313.

Wu, L. M., Lv, G. C., Liao, L. B., & Qin, F. X. (2015a). Stability and pH-independence of nano-zero-valent iron intercalated montmorillonite and its application on Cr(VI) removal. *Journal of Contaminant Hydrology, 179*, 1–9.

Wu, L. M., Lv, G. C., Liu, M., Li, Z. H., Liao, L. B., & Pan, C. F. (2015b). Adjusting the layer charges of host phyllosilicates to prevent luminescence quenching of fluorescence dyes. *Journal of Physical Chemistry C, 119*, 22625–22631.

Wu, L. M., Yang, C. X., Mei, L. F., Qin, F. X., Liao, L. B., & Lv, G. C. (2014b). Microstructure of different chain length ionic liquids intercalated into montmorillonite: A Molecular Dynamics Study. *Applied Clay Science, 99*, 266–274.

Wu, P., & Yan, X. P. (2010). A simple chemical etching strategy to generate "ion-imprinted" sites on the surface of quantum dots for selective fluorescence turn-on detecting of metal ions. *Chemical Communications, 46*, 7046–7048.

Xu, H., Miao, R., Fang, Z., & Zhong, X. (2011). Quantum dot-based "turn-on" fluorescent probe for detection of zinc and cadmium ions in aqueous media. *Analytica Chimica Acta, 687*, 82–88.

Yan, D. P., Lu, J., Ma, J., Qin, S., Wei, M., Evans, D. G., & Duan, X. (2011a). Layered host–guest materials with reversible piezochromic luminescence. *Angewandte Chemie International Edition, 50*, 7037–7040.

Yan, D. P., Lu, J., Ma, J., Wei, M., Evans, D. G., & Duan, X. (2011b). Reversibly thermochromic, fluorescent ultrathin films with a supramolecular architecture. *Angewandte Chemie International Edition, 50*, 720–723.

Yu, W. H., Zhu, T. T., Tong, D. S., Wang, M., Wu, Q. Q., & Zhou, C. H. (2017). Preparation of organo-montmorillonites and the relationship between microstructure and swellability. *Clays and Clay Minerals, 65*, 417–430.

Zhang, H., Cui, Z., Wang, Y., Zhang, K., Ji, X., Lu, C., Yang, B., & Gao, M. (2003). From water-soluble CdTe nanocrystals to fluorescent nanocrystal-polymer transparent composites using polymerizable surfactants. *Advanced Materials, 15*, 777–780.

Zhang, H., Wang, C., Li, M., Ji, X., Zhang, J., & Yang, B. (2005). Fluorescent nanocrystal-polymer composites from aqueous nanocrystals: Methods without ligand exchange. *Chemistry of Materials, 17*, 4783–4788.

Zhang, Z., Xu, B., Su, J., Shen, L., Xie, Y., & Tian, H. (2011). Color-tunable solid-state emission of 2,2′2Biindenyl-based fluorophores. *Angewandte Chemie International Edition, 123*, 11858–11861.

Zheng, M., Xie, Z., Qu, D., Li, D., Du, P., Jing, X., & Sun, Z. (2013). On-off-on gluorescent carbon dot nanosensor for recognition of Chromium(VI) and ascorbic acid based on the inner filter effect. *ACS Applied Materials & Interfaces, 5*, 13242–13247.

Zheng, Y., Orbulescu, J., Ji, X., Repoulos, F., Pham, S., & Leblanc, R. (2003). Development of fluorescent film sensors for the detection of divalent copper. *Journal of the American Chemical Society, 125*, 2680–2686.

Zhou, C. H., Zhao, L. Z., Wang, A. Q., Chen, T. H., & He, H. P. (2016). Current fundamental and applied research into clay minerals in China. *Applied Clay Science, 119*, 3–7.

Zhou, C. H., Zhou, Q., Wu, Q. Q., Jiang, X. C., Xia, S. T., Li, C. S., & Yu, W. H. (2019). Modification, hybridization and applications of saponite: An overview. *Applied Clay Science, 168*, 136–154.